Double electron capture and the angular distribution of ejected electrons in Ne^{8+}-He collisions

Z. Chen and C. D. Lin
Department of Physics, Kansas State University, Manhattan, Kansas 66506-2601
(Received 4 February 1993)

Double-electron-capture cross sections to individual doubly excited states and autoionizing electron spectra at fixed angles for Ne^{8+}- He collisions are calculated and analyzed for collision energies from 20 to 80 keV/amu. An independent-electron approximation is adopted where the amplitudes for double capture are derived from the antisymmetrized product of single-electron-capture amplitudes properly weighted with configuration-interaction coefficients. By choosing the quantization axis to be perpendicular to the collision plane, we also study the propensity rule for the M distribution of the cross section for each doubly excited state. The electron spectra at 0° are compared with experiments. At 80 keV/amu collision energy, our theoretical spectrum agrees with experiment very well. At lower energies, the agreements are not as good, but the dominant features are well predicted.

PACS number(s): 34.10.+x

I. INTRODUCTION

Double-electron-capture processes in collisions of multiply charged ions with atoms and molecules at low energies have been studied extensively in the past few years, in part due to the wide availability of highly charged ions, e.g., from electron-cyclotron-resonance and electron-beam ion sources in different laboratories. Experiments have been performed with many different ion projectiles, covering from fully stripped species to ions with a few core electrons and collision energies varying from a few keV/amu or less to about 100 keV/amu. Most high resolution experiments measure the spectra of the autoionizing electrons at a fixed angle [1–6]; experiments measuring x rays have also been carried out [7]. In general, the angular distributions of the ejected electrons or the photons are not measured except for a few cases. From the theoretical point of view, the double-capture process involves two active electrons. With highly charged ions as projectile, the two electrons are usually captured to high-lying doubly excited states where the principal quantum numbers of both electrons are relatively large. This means that a large number of states are populated in the collision. Although the close-coupling method appears to be the most appropriate approach for studying such collisions, the number of states to be included in such a calculation is very large and it is not realistic to carry out such calculations with present-day computers. Calculations of double-capture cross sections based on solving the two-electron Schrödinger equation in a close-coupling calculation have been limited to only low-lying doubly excited states, such as the $(2,2)$ doubly excited states [8,9]. Calculations beyond the $(2,2)$ manifold usually involve additional approximations. The molecular-orbital expansion method has been used to calculate the total cross section in low-energy collisions [10]. But this method has been used only to calculate the total cross section to each state. The cross sections to each magnetic substate are usually not correct. Thus a direct comparison of this calculation with the experimental spectrum is not possible. The classical overbarrier model and its variants have been used to estimate double-electron-capture cross sections, but the model has not been applied to state-selective partial cross sections. Recently, Posthumus, Lukey, and Morgenstern [11] considered the magnetic substate distribution using the classical overbarrier model. The model was shown to interpret fairly well the measured angular distributions for collisions of C^{6+} and O^{8+} on He, but poorly for O^{6+} and N^{5+} on H_2. Although the classical overbarrier model was expected to be valid for very low collision velocities, we will show that their model actually applies better to the velocity matching region.

Double differential cross-section measurements (in angles and energies) of N^{7+}, O^{8+}, Ne^{8+}, and other projectiles on He [12] showed that the scattering angles of the projectile in double electron capture are larger than those of single electron capture. This suggests that the two electrons could be captured sequentially where the projectile has to come closer to the target to capture the second electron. This two-step mechanism also suggests that the electron-electron correlation may not play a major role during the capture process, although it is crucial in describing each doubly excited state. In the collision of C^{6+}-He, the electron-electron correlation has been claimed to be important in double capture to the $(2,6)$ manifold [13]. But the total cross section of capture to the $(2,6)$ manifold is much smaller than that to the $(2,3)$ manifold. We do not expect the independent electron model to be applicable to weak processes.

Because of the slow collision velocities and the post-collision interaction effect, previous high-resolution experiments on double electron capture often do not separate each individual state very well within the (3,3), (3,4), and other manifolds. Recent experiments of Ne^{8+}- He by Raphaelian *et al.* [6] at relatively high collision energies

were able to distinguish most of these states. These data provide impetus to examine the validity of the independent electron model for double-capture processes at the state-selective level and calculations are made to compare the calculated ejected electron spectra with measured results. In this work we employ the independent-electron model to calculate the double-capture cross sections and the 0° electron spectra of Ne^{8+}- He collisions at relatively high collision energies, from 20 to 80 keV/amu [6] to assess the validity of this version of the independent electron model.

II. THEORETICAL MODEL

A. The independent-electron model

The time-dependent Schrödinger equation for a two-electron collision system is

$$\left[-\frac{1}{2}\nabla_1^2-\frac{1}{2}\nabla_2^2+V_P(r_1)+V_P(r_2)+V_T(r_1)+V_T(r_2)+\frac{1}{r_{12}}-i\frac{\partial}{\partial t}\right]\Phi(\mathbf{r}_1,\mathbf{r}_2,t)=0 \tag{2.1}$$

where $V_P(r)$ and $V_T(r)$ are the potentials of the projectile and target, respectively. In the velocity range of interest, the close-coupling method is the most suitable approach. However, the dominant double-capture process of Ne^{8+}- He collisions are to populate doubly excited states of the $(3,3)$ and $(3,4)$ manifolds. There are already 114 states if we consider only the doubly excited states in the $(3,3)$ and $(3,4)$ manifolds. To include also all the important single capture, excitation, and ionization channels, the number of states that need to be included in the close-coupling expansion will become prohibitively large. In addition, if the independent-electron model can describe the double-electron-capture process reasonably well, it will serve to support the two-step mechanism in a certain energy range for describing double-capture processes for certain systems of multiply charged ions colliding with atoms.

If the electron-electron interaction $1/r_{12}$ can be replaced by screening potentials, the two-electron two-center Schrödinger equation can be separated into two one-electron equations, which we can solve using, say, the close-coupling method. Thus, in this independent-electron model, the two-electron wave function can be written as the product of two one-electron wave functions [14,15]

$$\Phi(\mathbf{r}_1,\mathbf{r}_2,t)=\phi(\mathbf{r}_1,t)\phi(\mathbf{r}_2,t), \tag{2.2}$$

where the single-electron wave functions satisfy

$$\left[-\frac{1}{2}\nabla^2+V_P(r)+V_T(r)-i\frac{\partial}{\partial t}\right]\phi(\mathbf{r},t)=0. \tag{2.3}$$

In actual implementation, the model potentials of the projectile and the target in Eq. (2.3) are obtained by fitting to the experimental energy levels of $Ne^{7+}(1s^2nl)$ and $He(1snl)$, respectively. In our approach, $V_P(r)$ is chosen to be the same for each of the single-electron-capture processes while two different potentials $V_T(r)$ were used for the target. For the first electron a He model potential was used; for the second electron a pure Coulomb potential $-2/r$ was used. The use of different model potentials for the successive capture processes predicts that the dominant double-capture states are those in the $(3,3)$ and $(3,4)$ manifolds, consistent with data from O^{8+}- He and Ne^{8+}- He collisions. This is also inline with the classical overbarrier model, where the more tightly bonded electrons are allowed to relax. If a single He potential is used for both electrons, the dominant double capture will be mostly to the $(4,4)$ manifold, in disagreement with the experiments. To obtain single-electron-capture amplitudes, Eq. (2.3) is solved using two-center atomic orbitals in a close-coupling expansion at each impact parameter b. At the end of the collision, the one-electron wave function on the projectile can be expressed as

$$\phi(\mathbf{r},t\to\infty)=\sum_{n,l,m}a_{nlm}(b)\psi_{nlm}(\mathbf{r}) \tag{2.4}$$

where $\psi_{nlm}(\mathbf{r})$'s are the eigenfunctions of $Ne^{7+}(1s^2nlm)$. The two-electron wave function on the projectile after the collision is the (anti)symmetrized product of the two one-electron wave functions

$$\Phi(\mathbf{r}_1,\mathbf{r}_2,t\to\infty)=\mathcal{A}\sum_{n,l,m,n'l'm'}a_{nlm}(b)a'_{n'l'm'}(b)\times\psi_{nlm}(\mathbf{r}_1)\psi_{n'l'm'}(\mathbf{r}_2). \tag{2.5}$$

Since the initial total spin is zero, only singlet states are populated. This symmetrized wave function is then projected onto the eigenstates of $Ne^{6+}(1s^2nl,n'l')$, which are obtained by using the conventional configuration-interaction (CI) method. The modulus square of the amplitude gives the probability of populating a particular doubly excited state at impact parameter b. After integrating over the impact parameter plane, the total capture cross section to each doubly excited state is obtained.

B. The atomic parameters of doubly excited states

In constructing our CI wave functions for the doubly excited states of Ne^{6+}, we use the same one-electron orbitals (of Ne^{7+}) as those used for the basis functions in the close-coupling expansion. These basis functions are obtained by diagonalizing the single-electron Hamiltonian of Ne^{7+} using Slater-type orbitals. The two-electron basis functions are constructed by the (anti)symmetrized product of these one-electron basis functions with proper total angular momentum. The CI coefficients are determined by diagonalizing the Hamiltonian of the two-electron system

$$H = -\frac{1}{2}\nabla_1^2 - \frac{1}{2}\nabla_2^2 + V_P(r_1) + V_P(r_2) + \frac{1}{r_{12}}. \quad (2.6)$$

Table I gives the absolute values of the energy levels of $Ne^{6+}(1s^2 3l3l')$ and $Ne^{6+}(1s^2 3l4l')$ in order of increasing energies. The fluorescence yields for these states are essentially zero [4] so these doubly excited states will undergo autoionizing decay either to $Ne^{7+}(1s^2 2s)$ or $Ne^{7+}(1s^2 2p)$. This results in two groups in the emitted electron spectra separated by 16.02 eV, the energy difference between $Ne^{7+}(1s^2 2s)$ and $Ne^{7+}(1s^2 2p)$ states.

C. The "natural frame" coordinate system

Experimentally, it is convenient to choose the beam direction as the quantization axis. This is the most obvious coordinate system with cylindrical symmetry when the scattering angles of the projectile or the target are left unmeasured. But from the theoretical point of view, each collision event has a well-defined scattering plane and a more "natural" coordinate system is to choose the quantization axis to be perpendicular to the collision plane, defined by the incident direction and the vector of the scattered particle. In the semiclassical treatment as employed in our calculation, this scattering plane is defined by the beam velocity **v** and impact parameter **b**, as shown in Fig. 1. The x axis is along the direction of projectile velocity **v**; and the y axis along the impact parameter **b**; the quantization axis, the z axis, is along the direction perpendicular to the scattering plane. Using this coordinate system, it has been found that in the energy range where the collision velocity is comparable to the orbital velocity of the electron, the dominant magnetic substate populated is the $m = -l$ substate [16]. By constructing double-electron-capture amplitudes from single-electron-capture amplitudes with reference to the same quantization axis, it becomes very straightforward in predicting the dominant doubly excited states formed in these collisions. In actual calculation, the amplitudes are first calculated with the beam axis as the quantization axis. The amplitudes with respect to the natural frame are then obtained by a simple rotation.

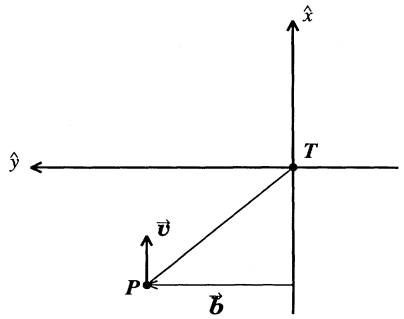

FIG. 1. The "natural" coordinate system. The x axis is chosen along the beam direction **v**, the y axis along the direction of impact parameter **b**, and the z axis, the quantization axis, is pointing out of the paper.

III. RESULTS

A. State-dependent double-capture cross sections at 80 keV/amu

To understand double-capture probability using the independent electron model, it is useful to examine first the single-electron-capture probabilities or amplitudes. In Fig. 2 we show the single-capture probabilities to individual magnetic substates, where the quantization axis is perpendicular to the scattering plane: (a) and (b) for electron capture to the $n = 3$ and $n = 4$ states for Ne^{8+}-He collisions and (c) and (d) for Ne^{8+}-He^+ collisions at 80 keV/amu collision energy. Note the vertical scale for Fig. 2(d) is much smaller than that for Fig. 2(c). So the second capture is mainly to $n = 3$ and the capture to $n = 4$ is negligible. Since the parity of the initial state is even, only those states with $l + m$ =even are populated. We only label those states with large capture probabilities, although all the states are included in the figure. One notices that for the two successive capture events, the dominant states populated are those with $m = -l$. The probabilities of populating the $m = -l + 2$ substates are much smaller. The first capture is mostly to $3p_{-1}$, $3d_{-2}$

TABLE I. Energies of doubly excited states of $Ne^{6+}(1s^2 3l, nl)$. States are ordered according to the energy in atomic units.

No.	$(3l, 3l')$	$-E$	No.	$(3l, 4l')$	$-E$	No.	$(3l, 4l')$	$-E$	No.	$(3l, 4l')$	$-E$
1	$^1S^e(1)$	7.078	1	$^1S^e(1)$	5.516	12	$^1D^o(2)$	5.224	23	$^1G^e(2)$	5.072
2	$^1D^e(1)$	6.833	2	$^1P^o(1)$	5.488	13	$^1S^e(2)$	5.203	24	$^1D^e(5)$	5.068
3	$^1P^o(1)$	6.825	3	$^1D^e(1)$	5.417	14	$^1D^e(3)$	5.198	25	$^1F^o(4)$	5.056
4	$^1D^o(1)$	6.664	4	$^1F^o(1)$	5.354	15	$^1F^e(2)$	5.196	26	$^1H^o(1)$	5.036
5	$^1S^e(2)$	6.630	5	$^1P^e(1)$	5.332	16	$^1G^o(1)$	5.172	27	$^1P^o(5)$	4.998
6	$^1D^e(2)$	6.618	6	$^1P^o(2)$	5.326	17	$^1P^e(2)$	5.164	28	$^1S^e(3)$	4.984
7	$^1F^o(1)$	6.470	7	$^1D^e(2)$	5.316	18	$^1G^e(1)$	5.163			
8	$^1G^e(1)$	6.440	8	$^1F^o(2)$	5.267	19	$^1D^o(3)$	5.118			
9	$^1D^e(3)$	6.386	9	$^1D^o(1)$	5.260	20	$^1D^e(4)$	5.115			
10	$^1P^o(2)$	6.376	10	$^1P^o(2)$	5.250	21	$^1F^o(3)$	5.111			
11	$^1S^e(3)$	6.168	11	$^1F^e(1)$	5.228	22	$^1P^o(4)$	5.078			

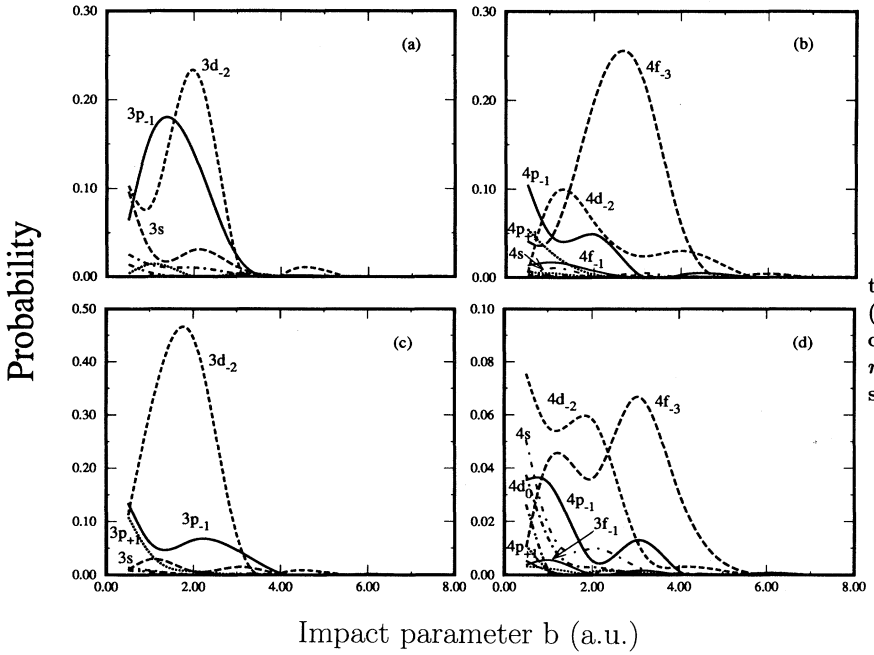

FIG. 2. Single-electron-capture probabilities at the collision energy of 80 keV/amu. (a) Ne^{8+}-He capture to $n = 3$; (b) Ne^{8+}-He capture to $n = 4$; (c) Ne^{8+}-He^{+} capture to $n = 3$; (d) Ne^{8+}-He^{+} capture to $n = 4$. Only substates with large probabilities are labeled.

[Fig. 2(a)], $4d_{-2}$, and $4f_{-3}$ [Fig. 2(b)], while the second capture is mostly to $3d_{-2}$ with a small portion of $3p_{-1}$ [Fig. 2(c)]. From the single-capture probabilities in Fig. 2, it is clear that the dominant double-capture channels will be the (3, 3) and (3, 4) manifolds. The total cross sections depend on the overlap of the probabilities in Figs. 2(a) and 2(c) for the (3, 3) manifold, or Figs. 2(b) and 2(c) for the (3, 4) manifold. Since the probabilities of capture to high-angular-momentum states with $m = -l$ are much larger than those of low-angular-momentum states, one expects immediately that doubly excited states with large magnetic quantum numbers $M = m_1 + m_2$ (with respect to the natural frame) are populated predominately. This in turn implies that high-angular-momentum doubly excited states are mostly populated in the collision. This conclusion can be drawn even without carrying out actual calculations. Note that it is not possible to make such a conclusion if the quantization axis is chosen to be along the beam direction where the probabilities for populating different magnetic states are comparable.

In Fig. 3, we give the total double-electron-capture cross section to each individual doubly excited state in both the (3, 3) and (3, 4) manifolds for collisions at 80 keV/amu. The cross sections are plotted according to the energies of doubly excited states, which are given in Table I. For example, the eleven states in the (3, 3) manifold are ordered as $^1S^e(1)$, $^1D^e(1)$, $^1P^o(1)$, $^1D^o(1)$, $^1S^e(2)$, $^1D^e(2)$, $^1F^o(1)$, $^1G^e(1)$, $^1D^e(3)$, $^1P^o(2)$, and $^1S^e(3)$ in increasing energies. For each state, we also indicate the cross sections for the magnetic substates. The shaded part is for $M_{\max}$, where $M_{\max} = -L$ if $\pi = (-1)^L$ and $M_{\max} = -L + 1$ if $\pi = (-1)^{L+1}$, the unfilled part represents the cross section for the $M = M_{\max} + 2$ substates, and so on. The cross section for all of the states are plotted, but some are too small to be seen. One notices

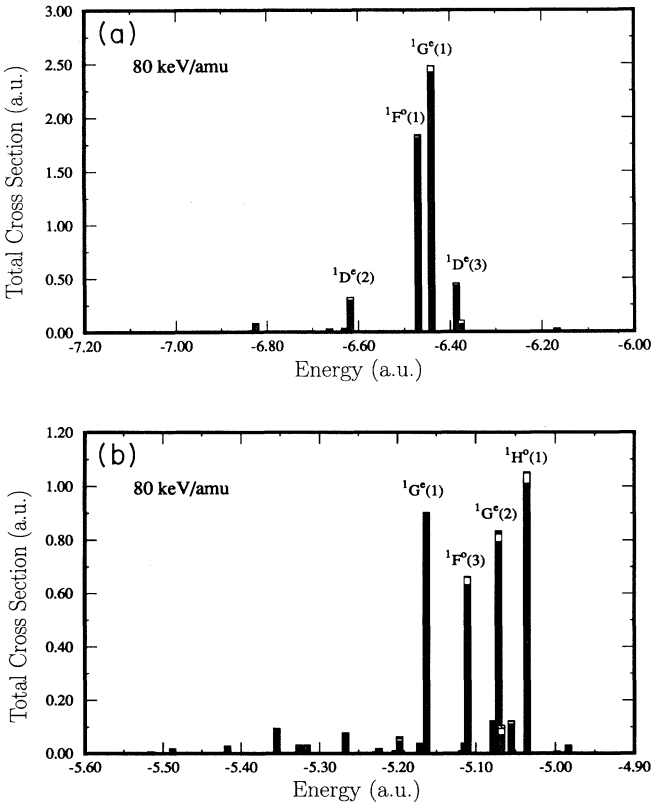

FIG. 3. Total double-electron-capture cross sections of Ne^{8+}-He to individual doubly excited states in (a) the (3, 3) manifold and (b) the (3, 4) manifold at the collision energy of 80 keV/amu. The shaded area is for $M = M_{\max}$ and the open area is for $M = M_{\max} + 2$ where $M_{\max}$ is defined in the text. All the other M components are essentially zero.

clearly that for each doubly excited state the dominant magnetic substate which has the largest double-electron-capture cross section (the shaded bars) is $M_{\max}$. There is a small contribution from $M_{\max}+2$. All the other M's are practically not populated. The propensity rule for single electron capture is thus reflected in the double-electron-capture process. Because of the propensity rule for single electron capture, the projection of the wave function to doubly excited states becomes much simpler. There is normally one dominant term plus other small terms. Since experiments usually do not measure the scattering angles of the projectile or the recoil target, information for the magnetic quantum number distribution is not obtainable directly from these experimental data.

From Fig. 2 we can easily understand why there are only two dominant peaks $^1F^o$ and $^1G^e$, the two states with the highest angular momenta, in the $(3,3)$ manifold [Fig. 3(a)]. These two states are mostly single configuration with

$$\begin{aligned} |^1F^o\rangle &= 0.983|3p3d\rangle + \cdots, \\ |^1G^e\rangle &= 0.986|3d3d\rangle + \cdots. \end{aligned} \tag{3.1}$$

The first single electron capture results in $3p_{-1}$ or $3d_{-2}$ substates and the second single electron capture is to $3d_{-2}$. The $3p_{-1}$ and $3d_{-2}$ substates couple to form $^1F^o$, while the two $3d_{-2}$'s give $^1G^e$. For the same reason, only those states with high angular momenta are populated in the $(3,4)$ manifold, $^1G^e(1)$, $^1F^o(3)$, $^1G^e(2)$, and $^1H^o(1)$ [Fig. 3(b)]. The cross sections of capture to $L \leq 2$ states are generally very small at this energy. The CI wave functions for the $^1F^o$, $^1G^e$, and $^1H^o$ states are given in the following:

$$|^1F^o(1)\rangle = 0.835|3s4f\rangle - 0.429|3p4d\rangle + 0.262|3d4p\rangle + 0.121|3d4f> + \cdots,$$

$$|^1F^o(2)\rangle = -0.432|3s4f\rangle - 0.596|3p4d\rangle + 0.597|3d4p\rangle - 0.276|3d4f\rangle + \cdots,$$

$$|^1G^e(1)\rangle = 0.786|3p4f\rangle - 0.542|3d4d\rangle + \cdots,$$

$$|^1F^o(3)\rangle = 0.067|3s4f\rangle + 0.582|3p4d\rangle + 0.720|3d4p\rangle + 0.220|3d4f\rangle + \cdots,$$

$$|^1G^e(2)\rangle = 0.524|3p4f\rangle + 0.792|3d4d\rangle + \cdots, \tag{3.2}$$

$$|^1F^o(4)\rangle = -0.211|3s4f\rangle - 0.272|3p4d\rangle - 0.055|3d4p\rangle + 0.887|3d4f\rangle + \cdots,$$

$$|^1H^o(1)\rangle = 0.943|3d4f\rangle + \cdots.$$

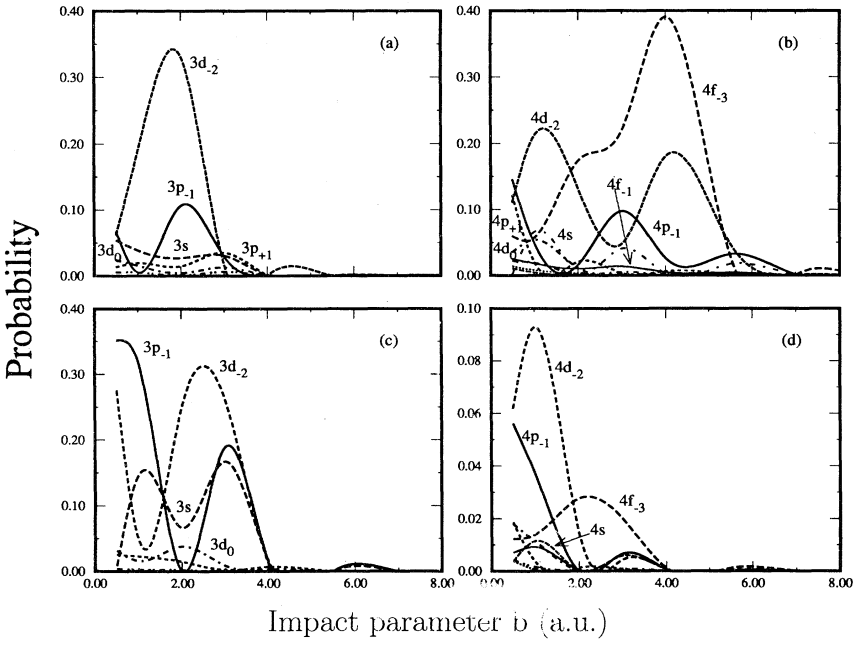

FIG. 4. The same as Fig. 2, but at 20 keV/amu collision energy.

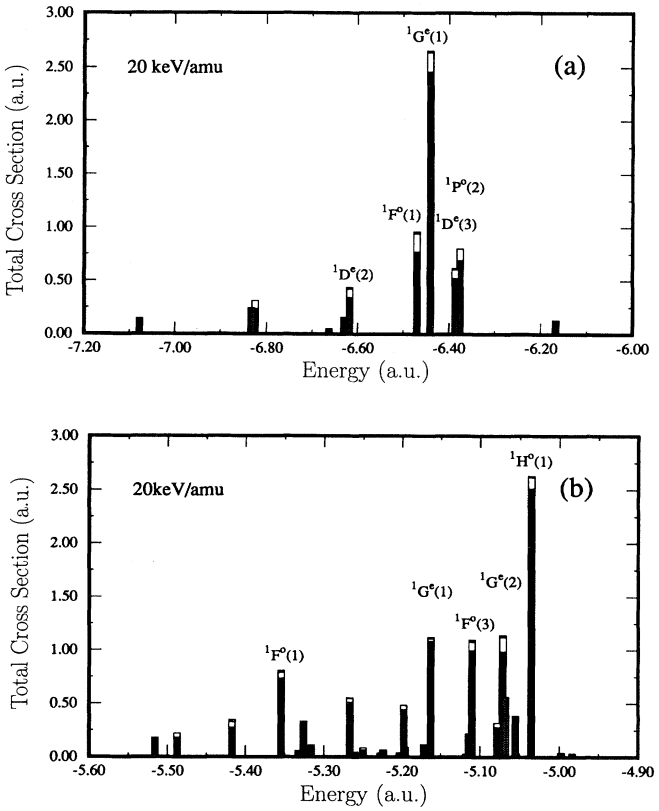

FIG. 5. The same as Fig. 3, but at 20 keV/amu collision energy.

Combined with Fig. 2 it is easy to see which states should be populated.

B. State-dependent double-capture cross sections at 20 keV/amu

At relatively higher collision energies, double electron capture populates preferentially high-angular-momentum states. When the projectile is moving relatively fast, the captured electron has no time to be recaptured by the target ion. This is reflected from the smooth capture probabilities versus impact parameters. Because capture occurs at large internuclear separation, the electron will gain a large angular momentum. As the collision energy decreases, the electron has time to oscillate between the projectile and target centers. This results in a relatively wide range of angular momentum for the captured electron and the capture probabilities oscillate versus impact parameters.

In Fig. 4 we show single-capture probabilities to $n = 3$ and $n = 4$ states versus impact parameters for both Ne^{8+}-He and Ne^{8+}-He^+ collisions at 20 keV/amu. As in the case at 80 keV/amu collision energy, the second single capture to $n = 4$ is negligible. The propensity rule still holds, though not as profound as at higher collision energies. We notice that there are more oscillations in the probabilities. We also notice that the probabilities of capturing to low-angular-momentum states are comparable to those of high-angular-momentum states, though they are still smaller. The probabilities for the first capture to $3p_{-1}, 3d_{-2}$, $4p_{-1}, 4d_{-2}$, and $4f_{-3}$ are the dominant ones [Figs. 4(a) and 4(b)]. For the capture from He^+, the probabilities to $3s, 3p_{-1}$, and $3d_{-2}$ are also of the same order [Fig. 4(c)]. Recall that double-electron-capture amplitudes are obtained by the product of the two successive single-electron-capture amplitudes properly weighted by the configuration-interaction coefficients. This means that there will be more states populated, as shown in Fig. 5, but the higher-angular-momentum states are still the preferred ones. Furthermore, states with $M_{\max}$ are dominantly populated, as seen by the dominance of the shaded area in each bar.

IV. EJECTED ELECTRON SPECTRA

A. Theoretical model

The doubly excited states formed in the double-capture process will decay either through autoionization or by emitting photons. Most experiments so far measure the autoionizing electron at fixed angles. In order to compare our theoretical calculations directly with experiments, we need to calculate the emitted electron spectra at fixed angles. For the doubly excited states formed in the capture process in Ne^{8+}-He collision, the radiative decay is negligible compared to the autoionizing decay [4]. Thus in our calculation, we take the fluorescence yield to be zero, meaning that there is no radiative stablization.

Due to the slow collision velocities, the doubly excited states formed in the collision autoionize in the electric field of the receding target ion. Because of this post-collision interaction (PCI), the position and the shape of the autoionizing electron spectra will undergo shift and broadening, respectively. There are several theoretical models to account for the PCI effect in the literature. In this work, we will follow van der Straten and Morgenstern [17], where the line shape for each individual state is given. At each impact parameter, or scattering angle of the projectile, the electron spectrum is then given by [2,18]

$$I(\theta) = 2\pi \sum_{n,l_1} \sum_{M} \left| \sum_{\alpha} f^{\alpha}(\varepsilon, \varepsilon_L) a^{\alpha}_{LM}(b) 4\pi \sum_{l_2} e^{i(\sigma_{l_2} + l_2\pi/2)} \langle \alpha LM \| V_A \| n l_1 \varepsilon_k l_2 \rangle \sum_{m_1 m_2} \langle l_1 l_2 m_1 m_2 | LM \rangle Y^*_{l_2 m_2}(\theta, \phi) \right|^2 , \quad (4.1)$$

where $a^{\alpha}_{LM}(b)$ is the double-capture amplitude to the doubly excited state $|\alpha LM\rangle$ [α denotes the approximate quantum numbers ${}_n(K,T)^A_N$] at impact parameter b, $f^{\alpha}(\varepsilon,\varepsilon_L)$ is the PCI line-shape function

$$|f^{\alpha}(\varepsilon,\varepsilon_L)| = \left(\frac{2q}{v\Gamma_r(1+\varepsilon_r^2)\sinh(\pi q/v)}\right)^{1/2} \times \exp\left\{\frac{\pi q}{2v}\left[1+\frac{2}{\pi}\tan^{-1}\left(-\frac{1}{\varepsilon-R}\right)\right]\right\}, \tag{4.2}$$

$$\arg(f) = -\frac{q}{v}\left[\ln\left(\frac{\Gamma_r}{2}\right)+\frac{1}{2}\ln(1+\varepsilon_r^2)\right] - \tan^{-1}\left(-\frac{1}{\varepsilon_r}\right) - \frac{\pi}{2} - \arg\left[\Gamma\left(1+i\frac{q}{v}\right)\right]$$

where Γ_r is the natural width, $\varepsilon_r = 2(\varepsilon-\varepsilon_L)/\Gamma_r$, $q = Q(1-v/|\mathbf{v}-\mathbf{v}_0|)$, Q the charge of the PCI inducer, $\mathbf{v}$ the velocity of the projectile, and $\mathbf{v}_0$ the velocity of the emitted electron in the emitter frame. One notices that the Stark effect, which mixes the neighboring resonance states, is not included in this PCI model.

In Eq. (4.1), the quantization axis is chosen to be along the beam direction, the same as that in the experiment. Since the scattering angle of the projectile was not measured, we need to integrate over the azimuthal angle ϕ and the impact parameters to obtain the electron spectra at each fixed angle θ. In our actual calculation of the decay amplitudes, we use the partial decay widths calculated by Bachau *et al.* [19], while the phases are calculated by us.

B. Ejected electron spectra at 80 keV/amu collision energy

In the collision of Ne^{8+}-He, the two electrons are mainly captured to the (3,3) and (3,4) manifolds. These doubly excited states undergo autoionizing decay to either $Ne^{7+}(1s^22s)$ or $Ne^{7+}(1s^22p)$. Since $Ne^{7+}(1s^22s)$ and $Ne^{7+}(1s^22p)$ states are separated by 16.02 eV, each manifold will result in two groups of peaks associated with decay to the two final states. In Fig. 6, we show the experimental electron spectra measured at zero degree [6] and the comparison with our theoretical electron spectra at 80 keV/amu collision energy. The theoretical spectrum has been convoluted according to the experimental resolution. The electron energy is measured from the emitter frame. In the theoretical spectrum, the energy shifts of the emitted electron due to the PCI effect are small at this collision energy. So they are not taken into account in our calculation.

There are four groups of peaks in the spectrum: (a) (30–54 eV), corresponding to $Ne^{6+}(1s^23l3l')$ states decaying to $Ne^{7+}(1s^22p)$; (b) (46–70 eV), corresponding to $Ne^{6+}(1s^23l3l')$ states decaying to $Ne^{7+}(1s^22s)$; (c) (72–87 eV), corresponding to $Ne^{6+}(1s^23l4l')$ decaying to $Ne^{7+}(1s^22p)$; and (d) (88–103 eV), corresponding to $Ne^{6+}(1s^23l4l')$ decaying to $Ne^{7+}(1s^22s)$, respectively. Because the decay of $Ne^{6+}(1s^23l5l')$ states to $Ne^{7+}(1s^22p)$ covers an energy range of 91–110 eV, overlapping with (d), the part of the spectrum above 90 eV becomes much more complicated and will not be considered further. The dominant groups of peaks are those decaying to $Ne^{7+}(1s^22p)$ because the average partial decay rate of these two manifolds is about five times larger than the decay to $Ne^{7+}(1s^22s)$.

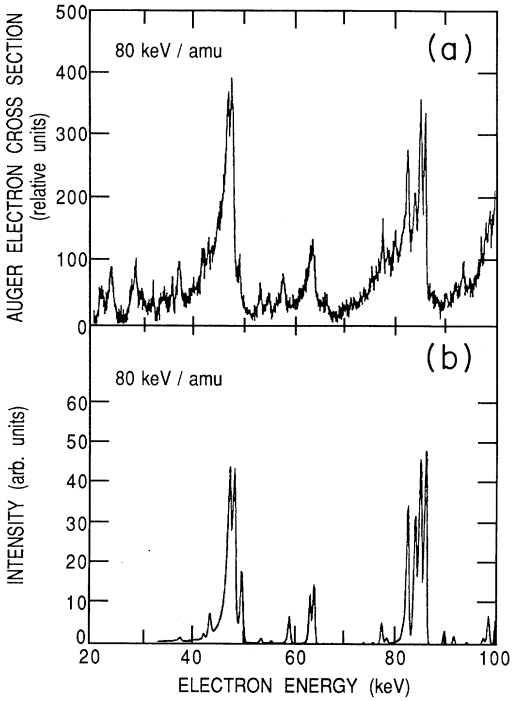

FIG. 6. (a) Experimental and (b) theoretical electron spectra at $\theta = 0°$ from the decay to $Ne^{6+}(1s^23l3l')$ and $Ne^{6+}(1s^23l4l')$ doubly excited states of Ne^{8+}-He collision at 80 keV/amu. The theoretical spectrum has been convoluted according to the experimental energy resolution. The electron energy is measured in the emitter frame.

From Fig. 6 we notice that the agreement between the theory and experiment is very good. At this collision energy, the PCI effect is not important and individual peaks are very well separated. The two large peaks at 47.1 and 48.0 eV correspond to the ${}^1F^o$ and ${}^1G^e$ states in the (3,3) manifold decaying to $2p$. The two small peaks at 43.1 and 49.4 eV on both sides of the large ones are ${}^1D^e(2)$ and ${}^1D^e(3)$, respectively. The four large peaks at 82.7, 84.1, 85.2, and 86.2 eV correspond to ${}^1G^e(1)$, ${}^1F^o(3)$, ${}^1G^e(2)$, and ${}^1H^o(1)$ states in the (3,4) manifold decaying to $2p$. For the weaker states, quantitative comparison becomes more difficult because of noises in the experimental signals. For the large peaks, even the relative heights, or the relative cross sections, also agree well with the experiment. The excellent agreement between the theoretical calculation using the independent-electron model and the experiment confirms that at this collision energy, electron

correlation does not play an important role in determining the formation of the dominant doubly excited states in the $Ne^{6+}(1s^2 3l3l')$ and $Ne^{6+}(1s^2 3l4l')$ manifolds, although it may be important for the very weak channels.

C. The angular dependence of the ejected electron spectra

Since the doubly excited states formed in the double-electron-capture process are in general aligned, we would expect a variation in the intensity of the electron spectra in different detecting angles. In Fig. 7 we plot the electron spectra of the (3,3) manifold at three different angles, $\theta = 0°$, 45°, and 90° measured in the emitter frame. The electron intensity is maximum at $\theta = 0°$ and minimum at $\theta = 90°$. The intensity of the $^1F^o$ and $^1G^e$ peaks is about twice as large at $\theta = 0^o$ than that at $\theta = 90°$. This can be understood from the M distribution in total cross sections of these states. In the coordinate system shown in Fig. 1, only the $M = -L$ components are populated, with a very small fraction of other M's (see Fig. 3). When we rotate the quantization axis to that of the beam direction, the $|M| = 0, 1$ components will be the dominant ones. The decay of these magnetic substates prefers $\theta = 0°$ [18]. We point out that the strong preference of the $M = -L$ component of the doubly excited states formed with respect to the quantization axis in the natural frame implies that the ejected electron will show strong orientation dependence if the scattering angles of the projectile or of the recoil ion are measured in coincidence with the angular distribution of the autoionizing electrons.

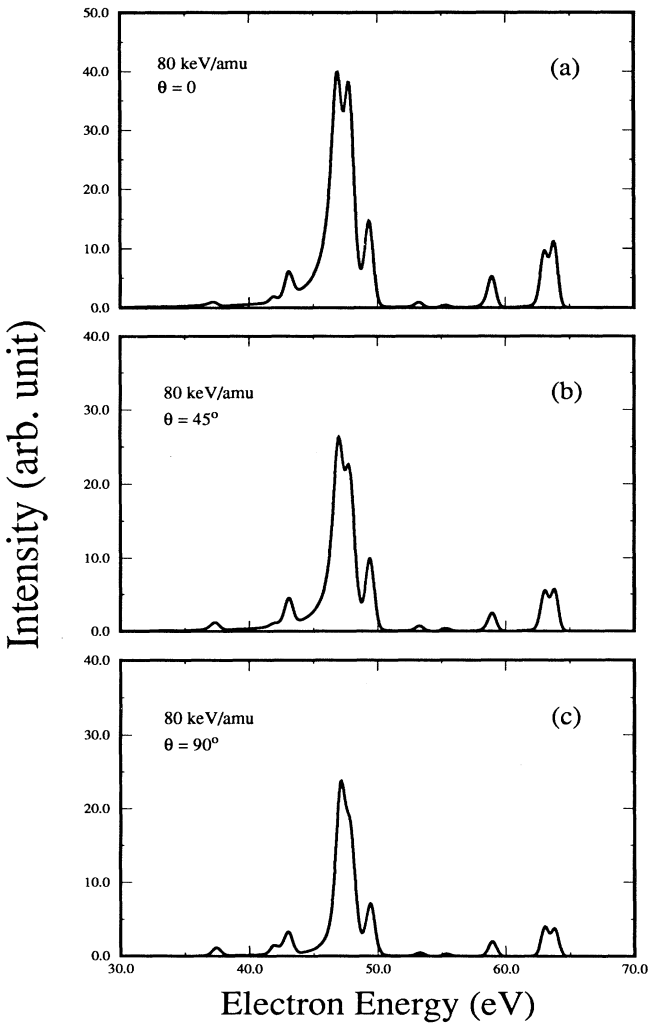

FIG. 7. Theoretical ejected electron spectra at different detecting angles from $Ne^{6+}(1s^2 3l3l')$ doubly excited states resulting from the collision of Ne^{8+}-He at 80 keV/amu collision energy.

D. Electron spectra at 20 keV/amu collision energy

In Fig. 8 we show the experimental electron spectrum [6] measured at 0° for incident energy at 20 keV/amu. Two theoretical spectra were calculated, one treating the electron spectrum from each doubly excited state coherently [Fig. 8(b)]. In order to show the effect of significant interference from different states at lower energies, we also carried out a calculation where the contribution from each doubly excited state to the spectrum is treated incoherently, and the result is shown in Fig. 8(c). One notices that the overall agreement between the theoretical and experimental spectra is still quite good. Comparing with the spectrum at 80 keV/amu, there are more peaks at this collision energy. The high peaks are still those associated with high angular momenta, but states with $L = 1, 2$ are also populated, though relatively weaker. The intensity of the states in the (3,4) manifold becomes significantly stronger than those in the (3,3) manifold, while at 80 keV/amu they are about the same. The $^1F^o$ and $^1G^e$ states decaying to $2p$ are still the largest peaks for the (3,3) manifold. The peak at 49.4 eV actually consists of the decay from two states $^1D^e(3)$ and $^1P^o(2)$. For the (3,4) manifold, in addition to the four major peaks between 82.7 eV and 86.2 eV similar to those observed at 80 keV/amu, an additional peak due to the decay of the $^1F^o(1)$ state at 77.5 eV becomes much more pronounced. These major features are identical to the experimental data. However, there are noticeable differences in the relative height of the peaks. For the (3,3) manifold, the two most pronounced peaks are those of $^1F^o$ at 47.1 eV and $^1G^e$ at 48.0 eV. In the experimental spectrum, Fig. 8(a), the $^1F^o$ intensity is higher than that of $^1G^e$, but the theoretical spectra shown in Fig. 8(b) gives opposite relative strength. The difference in the relative strength of the two peaks between the experiment and the theoretical calculation is actually due to the PCI effect according to the present calculation. To show this, we perform a calculation where the interference between the states is excluded. The electron spectrum from such an incoherent sum is shown in Fig. 8(c) where the relative intensity between the two peaks is seen to be in agreement with experiment. This PCI effect also affects the part of the

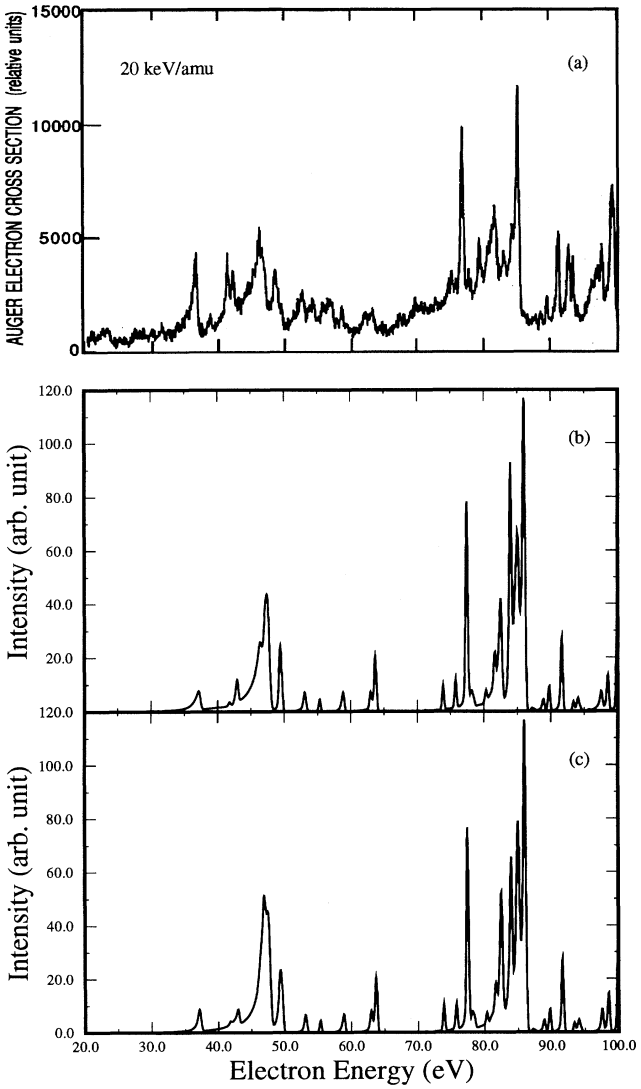

FIG. 8. The same as Fig. 6, but at 20 keV/amu collision energy. We also plot the theoretical spectrum shown in (c), assuming that there is no interference due to individual states.

spectrum corresponding to the (3, 4) manifold, though not as much as to the (3, 3) manifold, because the line widths are narrower in general for the states in the (3, 4) manifold.

V. SUMMARY AND CONCLUSIONS

In this paper, we have calculated and analyzed the state-selective double-electron-capture cross sections and the angular dependence of the resulting autoionizing electron spectra for Ne^{8+}-He collisions at energies of 20 to 80 keV/amu using the independent-electron approximation. The calculated electron spectra at 0° are in general agreement with experiments in that all the major peaks from the dominant doubly excited states populated are well reproduced in the calculation. At 80 keV/amu, the calculated relative electron intensities of the major peaks are also in agreement with experiment. At 20 keV/amu, the agreement is not as good in terms of the relative intensities, but the overall features of the spectra are also reproduced by the calculation. These results indicate that for the present collision system, the independent-electron approximation is capable of explaining the dominant doubly excited states formed in the double-electron-capture process, and that the electron-electron interaction does not play an essential role in the electron capture process, although electron correlation is explicitly included in the calculation of doubly excited states. The agreement between our theoretical spectra and experiment is less desirable for the collision energy at 20 keV/amu. At this energy, the post-collision-interaction effect is more important and the interference from neighboring states is significant. We have shown that the treatment of PCI effect can change the electron spectra at the lower energies and thus the disagreement between the theoretical calculation and experimental electron spectra can be due to the failure of the independent-electron model or the treatment of the PCI effect. Note that in the present model the post-collision effect of each state is treated separately. This is possible only if the states are well separated. In the present case, the energy separations between several neighboring states are smaller than the autoionization widths of the states and a more completed yet complicated treatment of the PCI effect is needed. Thus the discrepancy between theory and experiment cannot be attributed to the failure of the independent-electron approximation directly, although one expects that electron correlation to play a more important role for collisions at lower energies and for states with smaller cross sections.

By choosing the natural frame coordinate system where the quantization axis is perpendicular to the scattering plane, we have shown that states with $M = -L$ are strongly preferred in the double-capture process. This is the direct consequence of the propensity rule deduced from the single-electron-capture probabilities [16] and the independent-electron approximation. It is also shown that states with higher angular momenta are preferred. By studying the energy dependence, we also showed that doubly excited states with high-angular-momentum states are populated preferentially at higher energies, while states with lower angular momentum are also populated at lower energies. This propensity rule and angular momentum of the doubly excited states formed in the double-capture process was discussed in an extended classical over-barrier model by Posthumus, Lukey, and Morgenstern [11], but the model was designed for very low collision energies, in contradiction with the conclusion from our actual quantum-mechanical calculation.

ACKNOWLEDGMENT

This work was supported in part by the U.S. Department of Energy, Office of Basic Energy Sciences, Division of Chemical Sciences.

[1] A. Bordenave-Montesquieu, P. Benoit-Cattin, M. Boudjema, A. Gleizes, and H. Bachau, J. Phys. B **20**, L695 (1987).
[2] M. Mack, J. H. Nijland, P. v. d. Straten, A. Niehaus, and R. Morgenstern, Phys. Rev. A **39**, 3846 (1989).
[3] P. Moretto-Cappelle, D. H. Oza, P. Benoit-Cattin, A. Bordenave-Montesquieu, M Boudjema, A. Gleizes, S. Dousson, and D. Hitz, J. Phys. B **22**, 271 (1989).
[4] M. Boudjema, M. Cornille, J. Dubau, P. Moretto-Cappelle, A. Bordenave-Montesquieu, P. Benoit-Cattin, and A. Gleizes, J. Phys. B **24**, 1695 (1991); **24**, 1713 (1991).
[5] M. Barat and P. Roncin, J. Phys. B **25**, 2205 (1992), and reference therein.
[6] M. Raphaelian, G. Berry, N. Berrah, and D. Schneider, preceding paper, Phys. Rev. A **48**, 1292 (1993).
[7] A. Chetioui, M. F. Poltis, J. P. Rozet, A. Touati, L. Blumentfeld, D. Verhet, K. Wohrer, C. Stephan, M. Barat, M. N. Gaboriaud, H. Laurent, and P. Roncin, J. Phys. B **23**, 3659 (1990).
[8] W. Fritsch and C. D. Lin, Phys. Rev. A **45**, 6411 (1992).
[9] J. P. Hansen, A. Dubois, and S. E. Nielsen, Phys. Rev. A **45**, 184 (1992).
[10] C. Harel and H. Jouin, J. Phys. B **25**, 221 (1992), and references therein.
[11] J. H. Posthumus, P. Lukey, and R. Morgenstern, J. Phys. B **25**, 987 (1992).
[12] P. Roncin, M. Barat, and H. Laurent, Europhys. Lett. **2**, 371 (1986).
[13] N. Stolterfolt, C. C. Havener, R. A. Phaneuf, J. K. Swenson, S. M. Shafroth, and F. W. Meyer, Phys. Rev. Lett. **57**, 74 (1986).
[14] A. Jain, C. D. Lin, and W. Fritsch, Phys. Rev. A **39**, 1741 (1989).
[15] Z. Chen, R. Shingal, and C. D. Lin, J. Phys. B **24**, 4215 (1991).
[16] M. Lundsgaard and C. D. Lin, J. Phys. B **25**, L429, (1992).
[17] P. van der Straten and R. Morgenstern, Phys. Rev. A **34**, 4482 (1986).
[18] Z. Chen and C. D. Lin, J. Phys. B **24**, 4231 (1991).
[19] H. Bachau, P. Galan, F. Martín, A. Riera, and M. Yáñez, At. Data Nucl. Data Tables **44**, 305 (1990).